nature astronomy

Supplementary information https://doi.org/10.1038/s41550-024-02446-x

A swarm of dusty objects in orbit around the central star of planetary nebula WeSb 1

In the format provided by the authors and unedited

Supplementary information.

Table of contents:

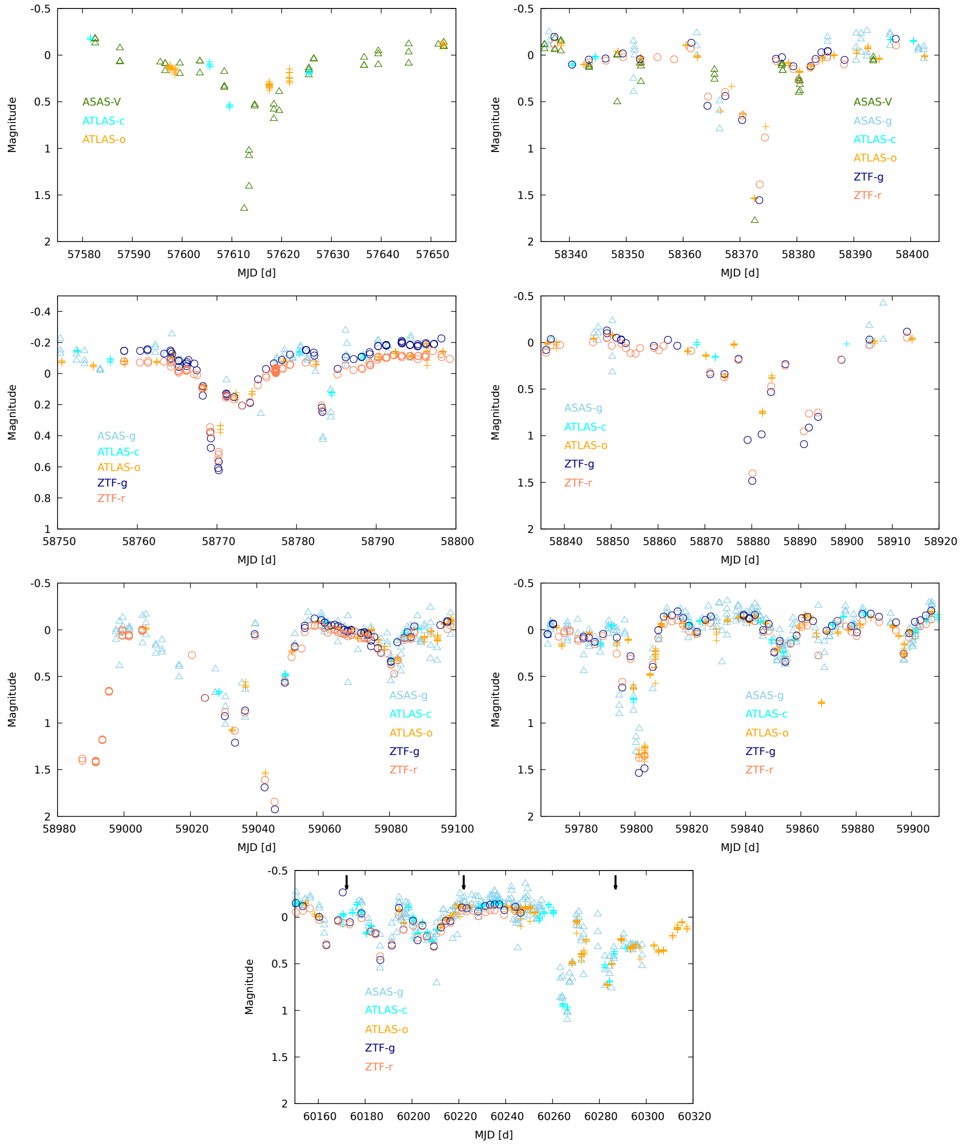

Supplementary Figure 1 Selected eclipse events in WeSb 1. ASAS-SN V - green triangles, g - sky-blue triangles; ZTF r - open orange circles, g - open navy-blue circles; ATLAS c - cyan plus signs, o -orange plus signs. Observations in the filters were offset by their median values. Black arrows indicate dates of our spectroscopic observations.

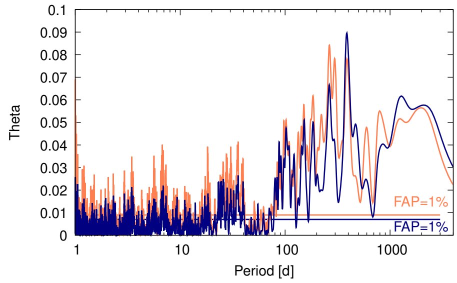

Supplementary Figure 2 Lomb-Scargle periodogram. All data in the visual domain -blue, ASAS data alone -orange. The two most pronounced peaks are at 390 and 260 days, respectively.

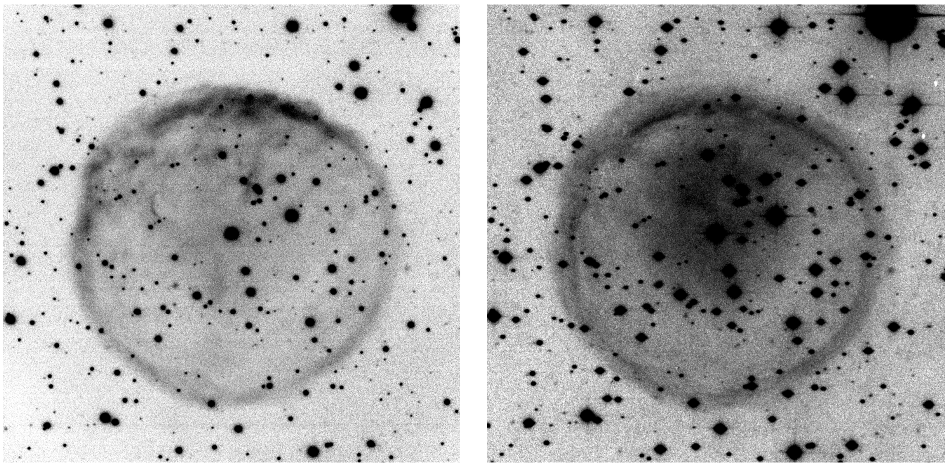

Supplementary Figure 3 Narrowband imaging of WeSb 1. Hα filter (left, NOT-ALFOSC) and [O III]5007 filter (right, combining data from both NOT-ALFOSC and INT-WFC). Each image measures 4'×4', North is up and East is left.

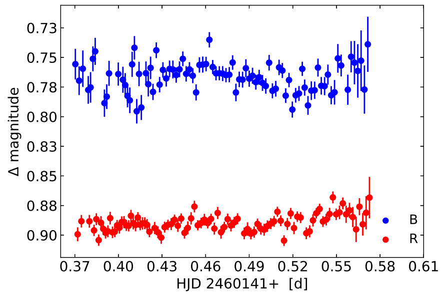

Supplementary Figure 4 Fast photometry during one night in two filters. Data are presented as mean values with SD error-bars.

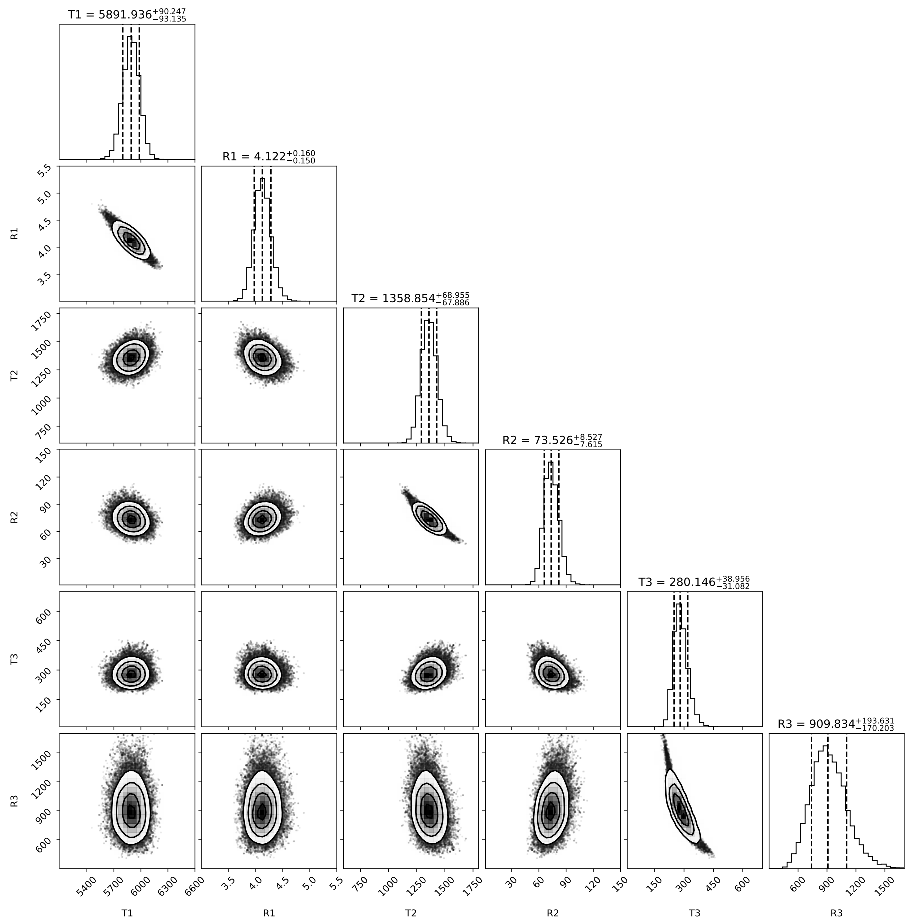

Supplementary Figure 5 The posterior probability distributions of the three black-body fit. Panels represent the uncertainties and correlations between the quantities.

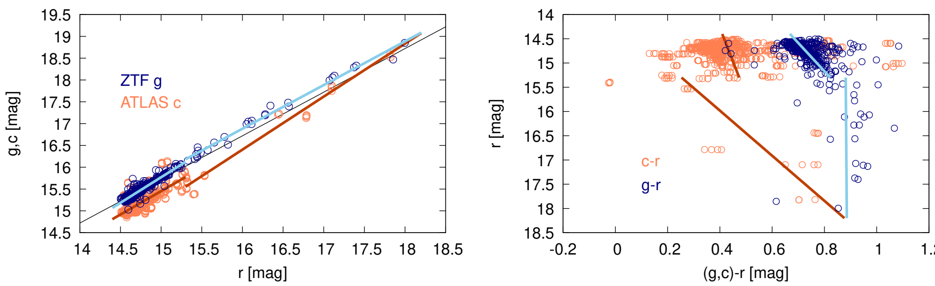

Supplementary Figure 6 Color dependence of eclipse events. Left: Brightness in ZTF g (navy-blue) and ATLAS c (orange) versus the combined red filter. The sky-blue lines are linear fits to (g, r) dependence for shallow and deep eclipses. Brown lines are linear fits to (c, r) dependence for shallow and deep eclipses separately. A thin black line represents the one to one dependence. Right: the combined red filter versus colour index $g - r$ (navy blue), $c - r$ (orange). The sky-blue and brown lines have the similar meaning.

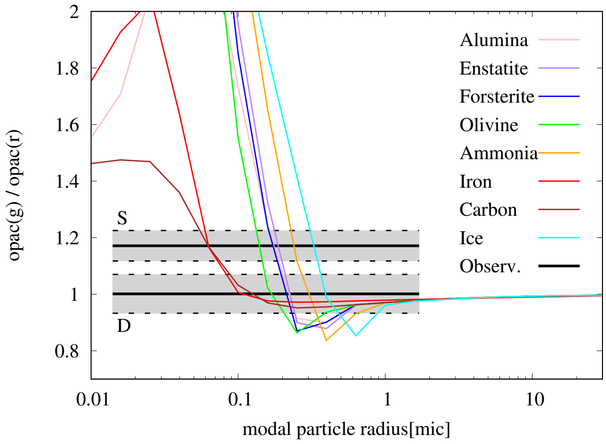

Supplementary Figure 7 Comparison of the observed and theoretical opacity ratios for ZTF g and combined red filters. Black solid horizontal lines are the mean values of the observed slopes for shallow (S) and deep (D) eclipses. Dashed horizontal lines mark the 3σ interval around them. Coloured lines depict the theoretical opacity ratios for the dust of different chemical composition as a function of the particle size.

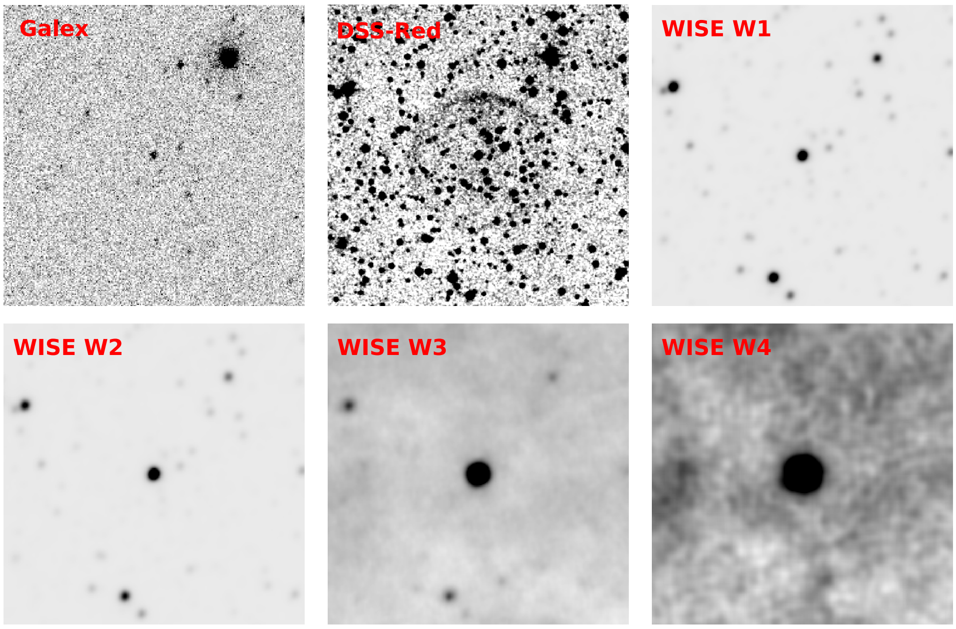

Supplementary Figure 8 PN WeSb 1 at different wavelengths. The central star is the brightest object at IR wavelength. The nebula itself is seen in DSS Red as a ring with the diameter of about 3' surrounding the nucleus. All images measure 6'×6'. North is up, East is left.

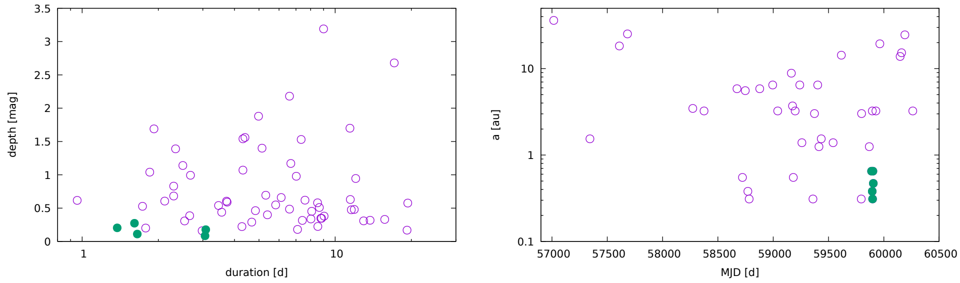

Supplementary Figure 9 Properties of the eclipse events and dust clouds. Left: Depths and duration of the eclipses. Right: Distance of the clouds from the G-subgiant. Full green circles mark the eclipses from the TESS sector No. 58.

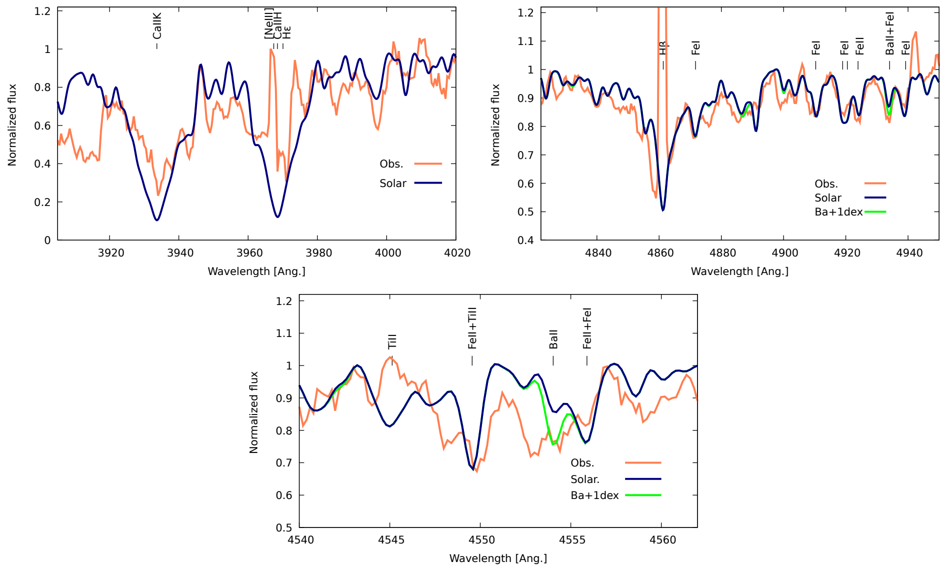

Supplementary Figure 10 Low resolution spectra of the optical light source. Left: Ca II lines. Right: Hβ region. Bottom: barium line region. Observations are in orange, synthetic spectrum for solar abundances in blue, and Ba enhanced by 1 dex in green.

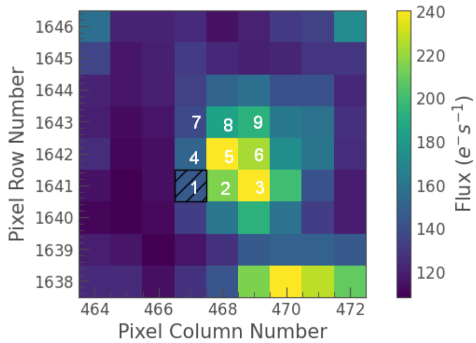

Supplementary Figure 11 TESS TPF. Our star is in pixel No.5.

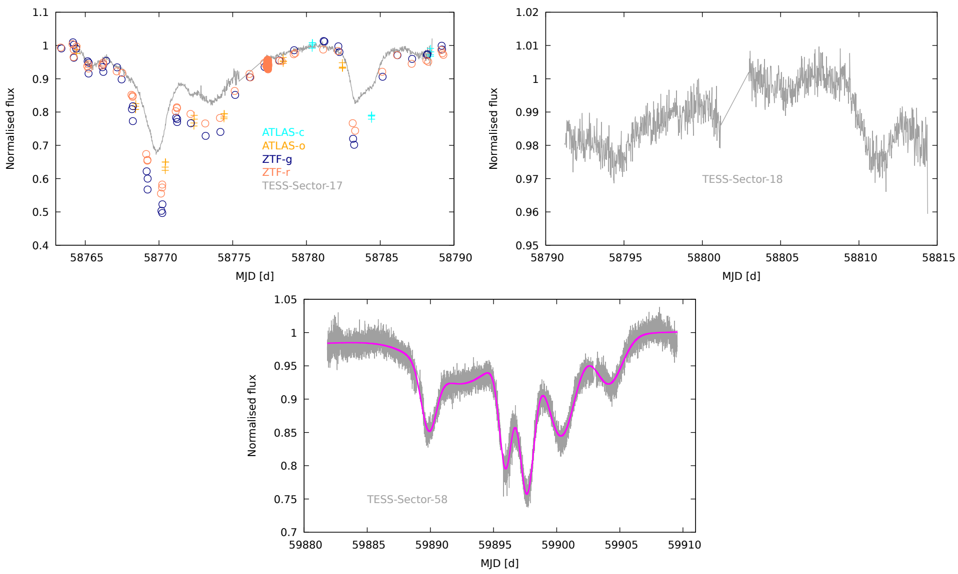

Supplementary Figure 12 TESS observations in three sectors. TESS data are shown as grey lines. Comparison with ZTF r data in sector 17 indicates that TESS amplitudes are reduced by a factor of 1.4 due to blending. Sector 18 is quiet. Sector 58 shows a chain of fast events and the fit to data (magenta line) involves 6 symmetric Gaussians.

Supplementary Table 1 Properties of spectral lines. First column is laboratory wavelength in air. Second column: radial velocity. Third column: fluxes integrated over the line profile relative to Hβ in %. Fluxes in Hβ are given at the bottom together with some line ratios. Fluxes with negative values indicate absorption features. Measurements are not corrected for the dust extinction. The last column contains the line identification.

	1st spectrum		2nd spectrum		3rd spectrum		
λ[Å]	v[km/s]	F/Fβ	v[km/s]	F/Fβ	v[km/s]	F/Fβ	Ident.
3868.71	-18.2	68.2			-15.5	52.6	[Ne III]
3967.41	-18.5	26.0			-16.5	22.2	[Ne III]
3970.07	-29.0	7.2					H5
4101.76	-19.8	16.7			-17.3	16.0	H4
4340.47	-19.4	34.9			-16.6	32.5	H3
4363.21	-21.2	81.0	-20.8	74.2	-21.7	82.1	[O III]
4685.70	-11.7	42.7	-20.9	44.8	-11.7	47.8	He II
4861.33	-18.7	100.0	-22.7	100.0	-21.4	100.0	Hβ
4861.33	-181.7	-6.2					Hβ far-blue abs.
4861.33	-92.2	-3.8			-100.5	-9.2	Hβ blue abs.
4958.92	-23.0	144.6	-21.2	157.5	-23.3	166.5	[O III]
5006.84	-22.0	440.7	-21.9	492.8	-22.5	519.4	[O III]
5754.64	-24.8	2.7					[N II]
5754.64	-72.3	-4.1					[N II] blue abs.
5875.67	-20.9	20.4			-22.3	24.5	He I
5889.95	-21.7	-19.4	-27.3	-29.0	-49.2	-14.1	Na I blue abs.
5895.92	-17.4	-14.3	-26.6	-21.0	-38.2	-9.8	Na I blue abs.
6435.11	-24.1	6.9					?[Ar V]
6562.82	-20.1	501.7	-20.8	511.0	-19.8	533.9	Hα
6562.82	-217.7	-25.0	-242.0	-35.6			Hα far-blue abs.
6562.82	-94.2	-4.7			-89.5	-12.8	Hα blue abs.
6678.15	-18.1	7.3					He I
7065.28	-21.9	13.5			-20.4	15.4	He I
7135.78	-21.8	8.3			-21.7	10.6	[Ar III]
Hβ		1.12		1.05		1.11	10^{-14} erg s^{-1} cm^{-2}
4363/Hγ		2.32				2.52	
5007/Hβ		4.41		4.93		5.19	

Supplementary Table 2 Properties of the star (PN nucleus). References: (1) -[1], (2) -[2], (3) -[3].

Property	value	Ref.
RA(2000)	01 00 54.1	1
DEC(2000)	+55 04 00.0	1
pmRA[mas/yr]	-1.278 ± 0.017	1
pmDEC[mas/yr]	-1.293 ± 0.018	1
Gaia G	14.77	1
Gaia BP	15.26	1
Gaia RP	14.09	1
Gaia BP-RP	1.17	1
$T_{\rm eff}$ [K]	5747	1
$\log g$ [cgs]	3.65	1
A(G)	0.58	1
E(BP-RP)	0.32	1
π [mas]	0.271 ± 0.024	1
Dist. [pc]	3690 ± 330	1
Dist. [pc]	3340 ± 280	2
RUWE	1.10	1
E(g-r)	0.26	3
A(g)	0.92	3
A(r)	0.68	3
E(B-V)	0.26	3

Supplementary Table 3 Coefficients of the linear fit of ZTF g and ATLAS c versus the combined red filter. The shallow region means shallow dips that are not deeper than r=15.3 mag. The deep region represent points fainter than r=15.3 mag. The full region covers all dips.

region	a_1	b_1
full	-0.63 ± 0.10	1.092 ± 0.007
shallow	-1.80 ± 0.26	1.171 ± 0.018
deep	$+0.86 \pm 0.37$	1.001 ± 0.023
region	a_2	b_2
full	-0.46 ± 0.24	1.060 ± 0.016
shallow	-0.63 ± 0.56	1.072 ± 0.038
deep	-3.03 ± 0.57	1.215 ± 0.035

Supplementary Table 4 Summary of our follow up observations. The MJD is the mid-point of the series of observations. Exposure duration is in minutes.

Date	MJD	Exposure	Telescope
		Imaging	
20230818	60175.192	3×12.5 [O III]	2.56m NOT
20230818	60175.220	3×12.5 Hα	2.56m NOT
20231007	60225.074	4×12.5 Hα	2.56m NOT
20231014	60231.992	3×12.5 [O III]	2.56m NOT
20231018	60235.162	3×20 [O III]	2.5m INT
20231019	60236.051	4×20 [O III]	2.5m INT
		Spectroscopy	
20230815	60172.102	3×15	2.56m NOT
20231004	60222.108	3×15	2.56m NOT
20231208	60286.949	3×15	2.56m NOT
		Photometry	
20230715	60140.970	292 B,R	1.3m SP

Appendix A PNe showing dust obscuration events

V651 Mon, which is a binary star and nucleus of the PN NGC 2346 [4], was eclipsed by a semi-transparent dust cloud for about 5 yr [5, 6]. The nucleus of PN M 2-29 showed a 3 yr long and one magnitude deep eclipse [7, 8] that is interpreted as due to circumbinary disk or an R Coronae Borealis (RCB) like event. CPD-56°8032 (V837 Ara) is a nucleus of PN Hen 3-1333 and has shown a series of pseudo-periodic dust occultation events that last for years, repeat approximately every 5 yr, and are more than 1 mag deep [8–11]. MPA 1746-3412 has a [WC10-11] Wolf-Rayet central star similar to PN Hen 3-1333 that shows a pseudo-periodic dimming on a time scale of 1000 days [12]. Perhaps most active PN is PHR 1806-2652. It shows numerous irregular clustered dips lasting a few months that are up to 2 mag deep [12]. Recently, a half a year long and one magnitude deep eclipse was discovered in the possible PN, PM 1-322 [13]. None of the above mentioned objects or events were associated with planets, smaller bodies, or their debris. However, the behavior of PHR 1806-2652 is similar to that of WeSb 1, although not that extreme. It would be interesting to revisit this object in the light or our results.

Appendix B Discussion of possible scenarios

Scenario (A): R Coronae Borealis-like (RCB-like) dust condensation. This process has been invoked before to explain obscuration events in a few PNe [e.g. 8]. In this scenario, a trigger (in the case of RCB, pulsations) generates stochastic shock waves that heat and subsequently cool the circumstellar medium via an adiabatic expansion followed by dust condensation along the line of sight that causes obscuration events [14, 15]. In the end, the dust cloud expands and disperses due to radiation pressure. This mechanism presumes carbon-rich and hydrogen-pure chemistry to generate dust in the form of carbon soot. RCB stars are pulsating F-G type supergiants with mas-loss rates that are much higher than those of our G-subgiant star, although we see a mass loss evidenced by P-Cyg profiles, which most likely originates from the CSPN. Fading events generated by this mechanism have a typical 'reverse nova' shape with a steep ingress, possible plateau, and a shallower egress that occur at irregular intervals and can last for months or years. Our events often show double, triple, and more complicated dips and their overall shapes do not agree with typical RCB-like events (individual dips are mainly symmetric events, see e.g. Sec. 5.9). We have no indications of pulsations, apart from a tentative 14 d period in SWASP data, and no indication of carbon in the spectra. Finally, this mechanism produces only small grains, typically 0.06 micron in size, while our dust clouds contain relatively large grains (>0.1 micron) with the exception of shallow dips that can indeed be explained by 0.06 micron carbon or iron grains. Consequently, we do not consider this scenario very likely.

Scenario (B): Symbiotic star. Spectra of symbiotic stars may sometimes resemble those of PNe. However, the circumstellar environment in symbiotic stars has typically much higher density than that found in PNe. A diagram of [O III]5007/Hβ versus [O III]4363/Hγ line ratios is often very convenient to distinguish between the symbiotic stars and PNe [16, 17]. Indeed, in this and similar diagrams, these line ratios lie in the same domain as D-type symbiotic stars. However, recall that our spectra are fiber-fed and observed emission lines originate from an unresolved nebula close to the star (see Sec. 5.6) rather than from the much larger surrounding PN. This unresolved nebula may have much higher density than the PN itself and might resemble PNe with high density cores [12]. Symbiotic stars usually contain a red giant star (S-type) or a variable Mira type star (D-type), but our SED is characterised by $T_1 = 5890\,K, R_1 = 4.1\,R_\odot$, which corresponds to a G-subgiant.

Such a G-subgiant might resemble the secondary star in another type of symbiotic stars, D'-type, which is a yellow giant. These stars have strong IR excess that peaks at wavelengths longer than 10 micron which is not our case. Yellow giants have low mass-loss rates which means that the PN would be a genuine PN composed of the material lost by the hot central star. These are very rare and the catalogue of symbiotic stars [18–20] lists only three cases of resolved nebulae around confirmed D'-type stars. The most reliable criterion for symbiotic stars is the presence of Raman scattered O VI 6825 and 7083 emission lines. These are not seen in our spectra. The apparently spherical geometry of our PN is not typical for nebulae of symbiotic stars that often feature bipolar outflows or other shapes. The angular size of our PN (180") would be record breaking for a symbiotic nebula [20]. Light curves of symbiotic stars are also very different from the variability seen in WeSb 1. To sum up, while we consider S or D-type symbiotic star scenario unlikely, it is not possible to exclude that it is a genuine PN harbouring 'an interacting binary' as e.g. indicated by strong barium lines in the G-subgiant star (Sec. 5.6).

Scenario (C): Optical double star. Here we explore the possibility that the PN is not related to the star experiencing the dusty eclipse events. We assume a background star (G-type subgiant), which is the major source of the continuum in the optical region, is also the star observed by Gaia, and which is eclipsed by the dust clouds. Then we have an unrelated CSPN that projects so close to the background star that it is unresolved. The CSPN shines mainly in the UV but is surrounded by the close unresolved nebula that is the source of the emission lines that we observe in the optical region. It has to be within about 1" from the background star so that it is not resolved by Galex nor our imaging. This would appear to be a particularly unlikely, nonetheless, there is precedence for such unlikely scenarios, for example, the A-type binaries discovered close to the projected centres of the PNe SuWt 2 and M3-2 have both been concluded to be chance alignments rather than real associations [the odds of which are less than 0.01%; 21, 22]. Similarly, the distance to the nebula, derived using the surface brightness-radius relationship of [23], is about 1.84±0.35 kpc – significantly closer than the Gaia distance of the optically bright source being eclipsed, although it must be stressed that this is a statistical distance which can be significantly wrong in individual cases.

In our case, the chances of such accidental alignment are significantly smaller than those mentioned above. It requires an uncommon and relatively bright star (G-type subgiant) with uncommon properties (strange variability) to spatially coincide with the CSPN. A small fraction of young stars (UXors, dippers) [24–26] may show such properties. However, they usually reside in clusters or associations and no open cluster is indicated within 20' from our star [27] and there are no other stars within 12'x12' field of view that are comparable or brighter in mid-IR W3 or W4 filters (see Sec. 5.3).

In the Gaia database we find 1086 stars equal or brighter than our star (G=14.8 mag) within 30' from our star. The likelihood that some of them would accidentally appear within 1" from our CSPN is about 3×10^{-4}. The probability that it is a young (< 10 Myr old) low mass star is an additional factor of 10^{-3} (assuming that most low mass stars spend about 10 Gyr on the main sequence). It should further be multiplied by a frequency of occurence of the UXor phenomena among young stars that we generously set to one. Assuming further that we searched among 2000 PNe, results in chances of such scenario of about 6×10^{-4}.

There are other arguments against this scenario. The emission lines originating from an unresolved nebula associated with CSPN can be used to trace it. They contribute 1-2% of flux to the broadband filters in the optical region. This means that our CSPN with its unresolved nebula would be about 4-5 mag fainter in the optical region than the background star, i.e. about 19 mag star. It is a lower limit on its brightness since the CSPN with the nebula might also slightly contribute to the optical continuum. Such a 19 magnitude CSPN might be detected by Gaia, which has a diffraction limit of about 0.1". However, the RUWE value is close to 1 and no such source is located within about 10" from the assumed background star (see Sec. 5.3). Finally, an indication of the enhanced Ba abundance of the G-subgiant (Sec. 5.6) suggests that this star has interacted with the CSPN. Hence, we consider this scenario unlikely but would like to encourage high-resolution (multi-band) imagery which could potentially resolve the CSPN from the background star.

Scenario (D): Inhomogeneous disk. This model presumes a circular, clumpy, edge-on Keplerian disk around our 1st SED component. It could also be a circumbinary disk but the absence of the reflection effect and presumed luminosity of the CSPN disfavour a short period binary (< 0.3 au) while the short duration of some eclipses indicate that the binary separation should not be larger than 0.3 au (see Secs. 5.9, 5.4), which does not leave much room for a compromise in this case. To put some constraint on the location of the dust clumps we explored in Sec. 5.4 the duration of the individual eclipses and of their ingress and egress. It resulted in upper limits of star-cloud separations within a broad interval of about 0.2-40 au. The luminosity of the G-subgiant and the condensation temperature of refractory dust (1500 K) place the inner edge of the disk at about 0.15 au (orbital periods of about 15 days) from the G-subgiant, which is close to where the innermost clouds are supposed to orbit. The parameters of the 2nd SED component from the Sec. 5.1 ($T_2 = 1360\,K, R_2 = 73\,R_\odot$) may in fact represent such an inner dusty disk. The tentative periodicities of 400 and 260 d would correspond to semi-major axes of 1.3 and 1.0 au, respectively.

The problem with this scenario is the nature of the disk and clumps. If the clumps were associated with more massive bodies on approximately edge-on circular orbits, such as planets or asteroids, one would expect a clear periodic nature of the events, which is not observed. In this particular case, such clouds would have to be transient features lasting only a few orbits, which would explain tentative 400 and 260 d periods. They might result from collisions with some other small bodies, or be associated with a second generation of planets being born, or temporal feeding of remnants of the first generation of planets with fresh material. However, it is also possible that 'clumps' are in fact some kind of temporary vertical disturbances, warps, waves, or eddies in the inner disk, perhaps caused by an interaction with a planet on an inclined or eccentric orbit, or an analogue of UXor like variability known from young stars [25].

Scenario (E): Disintegrating bodies. In this model, we assume the existence of numerous smaller bodies, such as exoasteroids or exocomets, on similar, long-period, and eccentric orbits. They could be orbiting the G-subgiant, CSPN, or both stars. However, the probability of eclipses in the circumbinary or circumCSPN scenarios significantly drop with the distance from the G-subgiant and may require a much more complicated geometry. These objects would represent the first generation of objects and their debris. Similar objects are postulated around Boyajian's star causing irregular eclipses with complex shapes [28, 29] or around ASASSN-21qj [30]. Such objects would be embedded in dust clouds made of large grains or debris, and would likely have a common progenitor. The Roche limit of the G-subgiant is well inside the star so the debris may result from a thermal disruption at large distances as observed in the Solar system [31]. They might also originate from mutual collisions, interaction with a disk, or from crossing of the water snow line. Assuming the luminosity of the G-subgiant (Sec. 5.1), grey opacity of water grains, and a condensation temperature of 150K, one gets its snow line at about 16 au.

If a body passes close to the CSPN, it might be tidally disrupted [32]. It was suggested that the tidal destruction of Earth-like planets or cores of icy planets might lead to the formation of smaller daughter planets [33, 34]. These are expected to form close to its Roche limit. Tidal destruction of a bigger and hydrogen rich gas giant planet followed by accretion of H-rich material may reignite the hydrogen on the surface of the compact star creating a so called 'real planetary nebula'. Our inner unresolved nebula might have originated this way. Dust and pebbles can also be created and accreted onto the rapidly dimming central star due to the purely non-gravitational effects such as Poyinting-Robertson and YORP effects [35]. Elliptical orbits also enhance the probability of eclipses which is higher during the periastron passage. The long period orbits of the postulated bodies could also explain the irregular nature of the dips. Such objects have never been detected during the PN or (post-)AGB stage, however, they are expected to occur following the AGB mass-loss phase [36, 37]. A proof of their existence during the WD stage of evolution is the metal contamination of WDs, their IR excess, and direct detections of exoplanets and exoasteroids orbiting WDs [38–44]. We consider this scenario and/or its combination with Scenario (D) as the most simple explanation of the WeSb 1 phenomenon.

Open questions: There are many open questions arising from this study. One of them is the separation between the CSPN and the G-subgiant star and whether the dust clouds are circumstellar, circumbinary, or circumCSPN. The central star system is unlikely to be a short period post-CE binary because of the large size of the G-subgiant, the lack of reflection effect or ellipsoidal variations in the light curve (see Sec. 5.9), projected spherical shape of the PN, and presumably higher luminosity of the CSPN. A wider binary is more likely. At least the dust clouds causing the fastest eclipses are likely orbiting the G-subgiant (Sec. 5.4). A70 is an example of CSPN that is a wide binary star with a G-subgiant barium secondary star. However, the properties of our PN even more resemble EGB 6 which is an ancient, large PN (2 pc), with nearly spherical shape, with a high density nebula, IR excess, and a distant companion [45].

HST was able to resolve the components and, surprisingly, the high density nebula and the IR excess were found to coincide with the companion star rather than the CSPN. The authors proposed that a portion of the wind from the AGB star was captured into an accretion disk around the companion star and survived to the present time. Note that PHR 1806-2652, the only PN that shows similar dust obscuration events to WeSb 1, also belongs to this rare category of high-density core PNe [12].

We propose a slightly different story, which might explain the EGB 6 phenomenon too: there was an AGB star orbited by numerous distant small rocky bodies and one more distant companion star (G-subgiant). The AGB star lost most of it mass, which destabilized orbits of the smaller bodies. In a binary, with the Roche lobe of AGB star shrinking and the lobe of G-subgiant expanding, a fraction of the bodies and dust material may wander from the former into the latter Roche lobe and even be focused into the orbital plane. As the AGB star turns into a hot CSPN it becomes very hostile for small bodies and dust that still happen to orbit close to it. However, 'our' bodies found safe harbour around the more distant G-subgiant where they can produce a debris disk and dust clouds. We are lucky since G-subgiant shines in the optical region and we can observe them eclipsing the star. This scenario would also answer the question why the variability was found in such an old, large, and low luminosity PN.

High resolution and multi-wavelength imaging might be very useful in that context. Far-UV or X-ray observations might detect the radiation from CSPN and constrain its properties. High resolution and high signal to noise optical spectroscopy of the G-subgiant would provide its radial velocities, chemical composition, and shed more light on its nature and its relation to the CSPN. The shape, size, density, chemical composition, radiation and brightness distribution, kinematics, interaction with the ISM, age of the PN, as well as the offset of the CSPN are yet to be explained and studied in more detail. Future high resolution spectroscopy of the PN itself will be crucial and might also shed more light on the properties of the CSPN. Potential variability of the HeII lines deserves further attention too.

References

[1] Gaia Collaboration *et al.* Gaia Data Release 3: Summary of the content and survey properties. *arXiv e-prints* arXiv:2208.00211 (2022).

[2] Bailer-Jones, C. A. L., Rybizki, J., Fouesneau, M., Demleitner, M. & Andrae, R. Estimating Distances from Parallaxes. V. Geometric and Photogeometric Distances to 1.47 Billion Stars in Gaia Early Data Release 3. *Astron. J.* **161**, 147 (2021).

[3] Green, G. M., Schlafly, E., Zucker, C., Speagle, J. S. & Finkbeiner, D. A 3D Dust Map Based on Gaia, Pan-STARRS 1, and 2MASS. *Astrophys. J.* **887**, 93 (2019).

[4] Brown, A. J., Jones, D., Boffin, H. M. J. & Van Winckel, H. On the post-common-envelope central star of the planetary nebula NGC 2346. *Mon. Not. R. Astron. Soc.* **482**, 4951–4955 (2019).

[5] Kohoutek, L. Central Star of Planetary Nebula NGC 2346: New Eclipsing Binary. *Information Bulletin on Variable Stars* **2113**, 1 (1982).

[6] Mendez, R. H., Gathier, R. & Niemela, V. S. The unprecedented light variations of NGC 2346. *Astron. Astrophys.* **116**, L5–L8 (1982).

[7] Hajduk, M., Zijlstra, A. A. & Gesicki, K. An occultation event in the nucleus of the planetary nebula M 2-29. *Astron. Astrophys.* **490**, L7–L10 (2008).

[8] Miszalski, B. *et al.* The influence of binarity on dust obscuration events in the planetary nebula M 2-29 and its analogues. *Astron. Astrophys.* **528**, A39 (2011).

[9] Pollacco, D. L., Kilkenny, D., Marang, F., van Wyk, F. & Roberts, G. The discovery of photometric variations in the prototype WC 11 star CPD -56 8032. *Mon. Not. R. Astron. Soc.* **256**, 669–672 (1992).

[10] Jones, A. *et al.* Long-term light curves for [WC] stars. *The Observatory* **119**, 76–80 (1999).

[11] Cohen, M., Barlow, M. J., Liu, X. W. & Jones, A. F. The dual dust chemistries of planetary nebulae with [WCL] central stars. *Mon. Not. R. Astron. Soc.* **332**, 879–890 (2002).

[12] Miszalski, B., Mikołajewska, J. & Udalski, A. Symbiotic stars and other Hα emission-line stars towards the Galactic bulge. *Mon. Not. R. Astron. Soc.* **432**, 3186–3217 (2013).

[13] Paunzen, E. *et al.* PM 1-322: New variable planetary nebula. *Astron. Astrophys.* **676**, A88 (2023).

[14] Goeres, A. & Sedlmayr, E. The envelopes of R Coronae Borealis stars. I. A

physical model of the decline events due to dust formation. *Astron. Astrophys.* **265**, 216 (1992).

[15] Woitke, P., Goeres, A. & Sedlmayr, E. On the gas temperature in the shocked circumstellar envelopes of pulsating stars. II. Shock induced condensation around R Coronae Borealis stars. *Astron. Astrophys.* **313**, 217–228 (1996).

[16] Iłkiewicz, K. & Mikołajewska, J. Distinguishing between symbiotic stars and planetary nebulae. *Astron. Astrophys.* **606**, A110 (2017).

[17] Gutierrez-Moreno, A., Moreno, H. & Cortes, G. A Diagnostic Diagram for Planetary Nebulae and Symbiotic Stars. *Publ. Astron. Soc. Pac.* **107**, 462 (1995).

[18] Merc, J., Gális, R. & Wolf, M. First Release of the New Online Database of Symbiotic Variables. *Research Notes of the American Astronomical Society* **3**, 28 (2019).

[19] Iłkiewicz, K., Mikołajewska, J., Miszalski, B., Kozłowski, S. & Udalski, A. A D'-type symbiotic binary in the planetary nebula SMP LMC 88. *Mon. Not. R. Astron. Soc.* **476**, 2605–2612 (2018).

[20] Corradi, R. L. M. Corradi, R. L. M., Mikolajewska, J. & Mahoney, T. J. (eds) *Large-Scale Ionized Outflows from Symbiotic Stars: A Real Link with Planetary Nebulae?* (eds Corradi, R. L. M., Mikolajewska, J. & Mahoney, T. J.) *Symbiotic Stars Probing Stellar Evolution*, Vol. 303 of *Astronomical Society of the Pacific Conference Series*, 393 (2003).

[21] Jones, D. & Boffin, H. M. J. On the possible triple central star system of PN SuWt 2: no ménage à trois at the heart of the Wedding Ring. *Mon. Not. R. Astron. Soc.* **466**, 2034–2038 (2017).

[22] Boffin, H. M. J. *et al.* When nature tries to trick us. An eclipsing eccentric close binary superposed on the central star of the planetary nebula M 3-2. *Astron. Astrophys.* **619**, A84 (2018).

[23] Frew, D. J., Parker, Q. A. & Bojičić, I. S. The Hα surface brightness-radius relation: a robust statistical distance indicator for planetary nebulae. *Mon. Not. R. Astron. Soc.* **455**, 1459–1488 (2016).

[24] Natta, A., Grinin, V. P., Mannings, V. & Ungerechts, H. The Evolutionary Status of UX Orionis-Type Stars. *Astrophys. J.* **491**, 885–890 (1997).

[25] Dullemond, C. P., van den Ancker, M. E., Acke, B. & van Boekel, R. Explaining UX Orionis Star Variability with Self-shadowed Disks. *Astrophys. J. Lett.* **594**, L47–L50 (2003).

[26] Ansdell, M. *et al.* Young "Dipper" Stars in Upper Sco and Oph Observed by K2.

Astrophys. J. **816**, 69 (2016).

[27] Hunt, E. L. & Reffert, S. Improving the open cluster census. II. An all-sky cluster catalogue with Gaia DR3. *Astron. Astrophys.* **673**, A114 (2023).

[28] Bodman, E. H. L. & Quillen, A. KIC 8462852: Transit of a Large Comet Family. *Astrophys. J. Lett.* **819**, L34 (2016).

[29] Neslušan, L. & Budaj, J. Mysterious eclipses in the light curve of KIC8462852: a possible explanation. *Astron. Astrophys.* **600**, A86 (2017).

[30] Marshall, J. P. *et al.* Sudden Extreme Obscuration of a Sun-like Main-sequence Star: Evolution of the Circumstellar Dust around ASASSN-21qj. *Astrophys. J.* **954**, 140 (2023).

[31] Granvik, M. *et al.* Super-catastrophic disruption of asteroids at small perihelion distances. *Nature* **530**, 303–306 (2016).

[32] Malamud, U. & Perets, H. B. Tidal disruption of planetary bodies by white dwarfs - II. Debris disc structure and ejected interstellar asteroids. *Mon. Not. R. Astron. Soc.* **493**, 698–712 (2020).

[33] Bear, E. & Soker, N. Planetary systems and real planetary nebulae from planet destruction near white dwarfs. *Mon. Not. R. Astron. Soc.* **450**, 4233–4239 (2015).

[34] Corradi, R. L. M., García-Rojas, J., Jones, D. & Rodríguez-Gil, P. Binarity and the Abundance Discrepancy Problem in Planetary Nebulae. *Astrophys. J.* **803**, 99 (2015).

[35] Veras, D., Birader, Y. & Zaman, U. Orbit decay of 2-100 au planetary remnants around white dwarfs with no gravitational assistance from planets. *Mon. Not. R. Astron. Soc.* **510**, 3379–3388 (2022).

[36] Debes, J. H. & Sigurdsson, S. Are There Unstable Planetary Systems around White Dwarfs? *Astrophys. J.* **572**, 556–565 (2002).

[37] Brouwers, M. G., Bonsor, A. & Malamud, U. A road-map to white dwarf pollution: tidal disruption, eccentric grind-down, and dust accretion. *Mon. Not. R. Astron. Soc.* **509**, 2404–2422 (2022).

[38] Vanderburg, A. *et al.* A disintegrating minor planet transiting a white dwarf. *Nature* **526**, 546–549 (2015).

[39] Manser, C. J. *et al.* A planetesimal orbiting within the debris disc around a white dwarf star. *Science* **364**, 66–69 (2019).

[40] Gänsicke, B. T. *et al.* Accretion of a giant planet onto a white dwarf star. *Nature* **576**, 61–64 (2019).

[41] Vanderbosch, Z. *et al.* A White Dwarf with Transiting Circumstellar Material Far outside the Roche Limit. *Astrophys. J.* **897**, 171 (2020).

[42] Vanderburg, A. *et al.* A giant planet candidate transiting a white dwarf. *Nature* **585**, 363–367 (2020).

[43] Blackman, J. W. *et al.* A Jovian analogue orbiting a white dwarf star. *Nature* **598**, 272–275 (2021).

[44] Guidry, J. A. *et al.* I Spy Transits and Pulsations: Empirical Variability in White Dwarfs Using Gaia and the Zwicky Transient Facility. *Astrophys. J.* **912**, 125 (2021).

[45] Bond, H. E. *et al.* The Nucleus of the Planetary Nebula EGB 6 as a Post-Mira Binary. *Astrophys. J.* **826**, 139 (2016).